Kinetics of the Unimolecular Decomposition of the 2-Chloroallyl Radical

Alexander A. Shestov,[†] Konstantin V. Popov,[‡] and Vadim D. Knyazev*

Research Center for Chemical Kinetics, Department of Chemistry, The Catholic University of America, Washington, D.C., 20064

Received: April 15, 2005; In Final Form: June 27, 2005

The thermal decomposition of the 2-chloroallyl radical, $CH_2CClCH_2 \rightarrow CH_2CCH_2 + Cl$ (1), was studied using the laser photolysis/photoionization mass spectrometry technique. Rate constants were determined in time-resolved experiments as a function of temperature (720−840 K) and bath gas density ([He] = (3−12) × 10^{16}, [N_2] = 6 × 10^{16} molecule cm^{-3}). C_3H_4 was observed as a primary product of reaction 1. The rate constants of reaction 1 are in the falloff, close to the low-pressure limit, under the conditions of the experiments. The potential energy surface (PES) of reaction 1 was studied using a variety of quantum chemical methods. The results of the study indicate that the minimum energy path of the CH_2CClCH_2 dissociation proceeds through a PES plateau corresponding to a weakly bound $Cl-C_3H_4$ complex; a PES saddle point exists between the equilibrium CH_2CClCH_2 structure and the $Cl-C_3H_4$ complex. The results of quantum chemical calculations, the rate constant values obtained in the experimental study, and literature data on the reverse reaction of addition of Cl to allene were used to create a model of reactions 1 and −1. The experimental dependences of the rate constants on temperature and pressure were reproduced in RRKM/master equation calculations. The reaction model provides expressions for the temperature dependences of the high-pressure-limit and the low-pressure-limit rate constants and the falloff broadening factors (at T = 300−1600 K): $k^{\infty}_1 = 1.45 \times 10^{20}T^{-1.75} \exp(-19609\ \mathrm{K}/T)\ s^{-1}$, $k^{\infty}_{-1} = 8.94 \times 10^{-10}T^{-0.40} \exp(481\ \mathrm{K}/T)\ cm^3\ molecule^{-1}\ s^{-1}$, $k_1^0(\mathrm{He}) = 5.01 \times 10^{-32}T^{-12.02} \exp(-22788\ \mathrm{K}/T)\ cm^3\ molecule^{-1}\ s^{-1}$, $k_1^0(N_2) = 2.50 \times 10^{-32}T^{-11.92} \exp(-22756\ \mathrm{K}/T)\ cm^3\ molecule^{-1}\ s^{-1}$, $F_{cent}(\mathrm{He}) = 0.46 \exp(-T/1001\ \mathrm{K}) + 0.54 \exp(-T/996\ \mathrm{K}) + \exp(-4008\ \mathrm{K}/T)$, and $F_{cent}(N_2) = 0.37 \exp(-T/2017\ \mathrm{K}) + 0.63 \exp(-\mathrm{T}/142\ \mathrm{K}) + \exp(-4812\ \mathrm{K}/T)$. The experimental data are not sufficient to specify all the parameters of the model; consequently, some of the model parameters were obtained from quantum chemical calculations and from analogy with other reactions of radical decomposition. Thus, the parametrization is most reliable under conditions close to those used in the experiments.

Introduction

Kinetic modeling of processes such as the combustion and incineration of chlorinated hydrocarbons and industrial chlorination is essential for understanding their mechanisms and for the use of these mechanisms as tools of prediction and control. The success of such modeling is currently limited by a lack of fundamental information on the rates and products of a large number of elementary reactions involving chlorinated hydrocarbon species.[1−3]

Resonantly stabilized (due to electron delocalization) radicals are known to play an important role in the chemical mechanisms of hydrocarbon oxidation and pyrolysis. The stability and low reactivity of these radicals result in their accumulation in large concentrations during the processes of oxidation and pyrolysis of hydrocarbons. High concentrations of stabilized polyatomic radicals result in appreciable rates of their recombination, ultimately leading to molecular growth, which has been linked to the formation of polycyclic aromatics and soot. In the oxidation and pyrolysis of chlorinated hydrocarbons, chlorinated delocalized radicals can be expected to play a role similar to the role of delocalized radicals in hydrocarbon combustion. Molecular weight growth due to the buildup and recombination of delocalized chlorinated hydrocarbon radicals is likely to produce aromatic and chlorinated aromatic species characterized by high toxicity and carcinogenicity (e.g., refs 2 and 4). The principal issue pertaining to the ability of such radicals to accumulate in combustion systems is their stability. In particular, the rates of the two most important processes of radical removal, reactions with O_2 and unimolecular decomposition, are the most critical parameters that determine the stability of radicals in flames.

Virtually no information is currently available in the literature on the kinetics of these reactions of delocalized chlorinated hydrocarbon radicals at elevated temperatures. In a recent direct, time-resolved experimental study, we investigated the kinetics and thermochemistry of the reaction of one of the simplest delocalized chlorinated hydrocarbon radicals, the 2-chloroallyl radical, with molecular oxygen.[5] The kinetics of the thermal decomposition of CH_2CClCH_2, however, remains unknown: no experimental information on this reaction is currently available in the literature.

In this article, we report the results of our experimental and computational investigation of the reaction of the thermal unimolecular decomposition of the 2-chloroallyl radical

$$CH_2CClCH_2 \rightarrow CH_2CCH_2 + Cl \qquad (1)$$

Reaction 1 was studied in the 720−840 K temperature interval at varying densities of helium bath gas ([He] = (3−12) × 10^{16}

[†] Current address: Center for Magnetic Resonance Research, University of Minnesota, Minneapolis, MN 55455.

[‡] On leave from the Higher Chemical College of the Russian Academy of Sciences, Miusskaya sq, 9, Moscow 125190, Russia.

10.1021/jp051968q CCC: $30.25 © 2005 American Chemical Society
Published on Web 08/18/2005

atom cm^{-3}) and at one density of nitrogen bath gas ($[N_2] = 6 \times 10^{16}$ molecule cm^{-3}). Rate constants were obtained as functions of temperature and bath gas density. In the computational part of the work, the potential energy surface (PES) of reaction 1 and the reverse reaction,

$$Cl + CH_2CCH_2 \rightarrow CH_2CClCH_2 \qquad (-1)$$

was studied using a variety of quantum chemical techniques. A model of the reactions (1, −1) was created on the basis of the results of the PES study and the experimental data obtained in the current work (reaction 1) and earlier studies (reaction −1). The experimental dependences of the rate constant (k_1 and k_{-1}) on temperature and pressure were reproduced in RRKM/master equation calculations. The model was used to obtain parametrized expressions for the rate constants as functions of pressure and temperature over wide ranges of conditions.

Reaction 1 has not been studied experimentally before. However, the kinetics of the reverse reaction (−1) has been studied by several groups. Wallington et al.[6] used a relative rates technique to obtain the rate constant of reaction −1 at 295 K and 760 Torr of nitrogen bath gas, where the reaction is near its high-pressure limit. Farrell and Taatjes[7] used a laser photolysis/IR absorption method to study the production of HCl in the reaction of Cl with allene. Although these authors were primarily interested in the channel of the $Cl + CH_2CCH_2$ reaction producing HCl and the propargyl radical, their experimental data (covering the temperature range from 292 to 850 K and two pressures of the CO_2 bath gas, 5 and 10 Torr) include both the rate constants for the overall reaction and those for the HCl producing channel. Rate constants for the other channel, reaction −1, can thus be extracted from these data. Finally, Atkinson and Hudgens[8] obtained the rate constants of reaction −1 at 298 K and low pressures (5−10 Torr) of He and N_2 bath gases in cavity ring-down spectroscopy experiments. Computational quantum chemical studies of the PES and the mechanism of reaction −1 were performed by Atkinson and Hudgens[8] and Hudgens and Gonzalez.[9]

This article is organized as follows. Section I is an introduction. The experimental study is described in section II. Section III presents a PES quantum chemical computational study, RRKM/master equation modeling of the reaction, and a parametrized representation of the calculated rate constants over wide ranges of temperatures and pressures. A discussion of the experimental and the computational results is given in section IV.

II. Experimental Study and Results

II.1. Experimental Apparatus and Method. 2-Chloroallyl radicals were produced by the pulsed, 193-nm laser photolysis of 2,3-dichloropropene. The decay of C_3H_4Cl ($m/z = 75$) was subsequently monitored in time-resolved experiments using photoionization mass spectrometry. Details of the experimental apparatus[10] and procedures[11] used have been described before and thus are only briefly reviewed here.

Pulsed unfocused 193-nm radiation (4 Hz) from a Lambda Physik EMG 201MSC excimer laser was directed along the axis of a heatable quartz reactor (1.05-cm-i.d.) coated with boron oxide.[12] Gas flowing through the tube at ≈4 m s^{-1} contained the radical precursor (≤0.01%) and an inert carrier gas (He or N_2) in large excess. The flowing gas was completely replaced between laser pulses. Gas was sampled through a hole (0.04 cm diameter) in the side of the reactor and formed into a beam by a conical skimmer before the gas entered the vacuum chamber containing the photoionization mass spectrometer. As the gas beam traversed the ion source, a portion was photoionized and mass selected. CH_2CClCH_2 radicals were ionized using the light from a chlorine resonance lamp (8.9−9.1 eV) with a CaF_2 window. Temporal ion signal profiles were recorded on a multichannel scaler from a short time before each laser pulse up to 25 ms following the pulse. Typically, data from 1000 to 20 000 repetitions of the experiment were accumulated before the data were analyzed.

The 193 nm photolysis of 2,3-dichloropropene can be expected to yield the following potential channels:

$$CH_2CClCH_2Cl \xrightarrow{193\ nm} CH_2CClCH_2 + Cl \qquad (2a)$$

$$\rightarrow CH_2CCH_2Cl + Cl \rightarrow CH_2CClCH_2 + Cl \qquad (2b)$$

$$\rightarrow CH_2CHCHCl + Cl \qquad (2c)$$

$$\rightarrow \text{other products} \qquad (2d)$$

This distribution of channels is consistent with the observed kinetics of the C_3H_4Cl radicals formed and with the results of quantum chemical studies of C_3H_4Cl, as explained below. Channel 2a results from the elimination of a chlorine atom from the chloromethyl group of 2,3-dichloropropene. Channel 2b, elimination of a Cl atom from the middle carbon in 2,3-dichloropropene, is also possible. This would result in the formation of a vinylic CH_2CCH_2Cl radical. Recent experimental[7,8] and theoretical[7−9] studies of the reaction of Cl atoms with allene and the associated potential energy surfaces demonstrate that CH_2CCH_2Cl is unstable and undergoes rapid isomerizations to 2-chloroallyl radical. Thus, the ultimate products of channel 2b are expected to be the same of those of channel 2a, $CH_2CClCH_2 + Cl$. The photolysis channel 2c forming the 1-chloroallyl radical (see discussion below) requires a prior isomerization of the excited 2,3-dichloropropene molecule.

Below 600 K, a slow exponential decay of the C_3H_4Cl ion signal was observed with the first-order rate constants in the range 12−28 s^{-1}, independent of temperature. This decay was attributed to a first-order heterogeneous wall-loss process:

$$CH_2CClCH_2 \rightarrow \text{heterogeneous loss} \qquad (3)$$

The rates of heterogeneous loss of CH_2CClCH_2 demonstrated a relatively minor instability: the values of k_3 slowly increased during the experiments. One possible reason for such an increase is that the Cl atoms formed in the precursor photolysis decayed on the walls of the reactor and affected the wall conditions, making the walls more reactive toward hydrocarbon radicals. To avoid effect of the chlorine atoms on the wall conditions, the former were converted to HCl and C_2H_5 by addition of ethane. When substantial concentrations ($(1.35-3.12) \times 10^{15}$ molecule cm^{-3}) of ethane were added to the reactor gas flow, the values of k_3 became stable.

Above 700 K the decay rates increased rapidly with rising temperature due to the increasing importance of the thermal decomposition of CH_2CClCH_2 radical, reaction 1. However, the C_3H_4Cl ion signal profiles displayed nonexponential profiles that could be represented with a double-exponential decay function:

$$I(t) = I_1 \exp(-k't) + I_2 \exp(-k_5 t) \qquad (I_2 \approx 0.13 I_1) \quad (I)$$

Thus, the ion signal at $m/z = 75$ (C_3H_4Cl) consisted of two components, the major one of which (first term in eq I) decayed

with time in a manner consistent with the thermal decomposition of a radical (decay rate k' increased with temperature and pressure); this component was attributed to the 2-chloroallyl radical. The minor component of the ion signal displayed a slow decay consistent with a heterogeneous wall loss of a radical. The rate constant k_5 of this decay did not increase with temperature in the 700−1000 K interval and coincided with that obtained in separate experiments for the $CH_2CHCHCl$ radical produced in the 193 nm photolysis of the $CHClCHCH_2$-$Si(CH_3)_3$ precursor:

$$CHClCHCH_2Si(CH_3)_3 \xrightarrow{193\ nm} CH_2CHCHCl + Si(CH_3)_3 \quad (4a)$$

$$\rightarrow \text{other products} \quad (4b)$$

This minor component was thus attributed to 1-chloroallyl radical, $CH_2CHCHCl$, which can be expected to have a significantly larger energy barrier for dissociation and thus to be thermally stable in the temperature range of the current experimental study. Its decay was thus attributed to a heterogeneous loss:

$$CH_2CHCHCl \rightarrow \text{heterogeneous loss} \quad (5)$$

The $C_3H_4Cl^+$ ion signal decay profiles were analyzed by fitting with eq I. The rate constants of the heterogeneous loss of CH_2CClCH_2, k_3, were directly determined below 600 K. For each experiment to determine k_1, the value of k_5 was obtained in a separate experiment performed under the same conditions (temperature and pressure), where small concentrations of 1-chloroallyl radicals ($\leq 2 \times 10^{11}$ molecule cm^{-3}) were created by the photolysis of $CHClCHCH_2Si(CH_3)_3$, reaction 4. The fitting of the $C_3H_4Cl^+$ ion signal decay profiles with eq I was performed by optimizing the values of three variables: (1) the maximum signal amplitude I_0 ($I_0 = I_1 + I_2$), (2) the ratio F_R of the initial intensities of the two components of eq I ($F_R = I_2/I_1$), and (3) the rate constant of the decay of the first component, k'. The values of k_1 were obtained by subtracting the rate of the heterogeneous loss of CH_2CClCH_2: $k_1 = k' - k_3$. A typical $C_3H_4Cl^+$ signal profile is presented in Figure 1.

Experiments were performed to establish that the rate constants did not depend on the initial radical concentration, the concentration of the radical precursor (provided that these concentrations were kept low enough to ensure that radical−radical reactions had negligible rates), the concentration of ethane, or the photolyzing laser intensity. The rate constants of the CH_2CClCH_2 decomposition depended only on temperature and bath gas density.

Possible side reactions of CH_2CClCH_2, $CH_2CHCHCl$, and C_2H_5 (other than reactions 1, 3, and 5) were considered from the standpoint of potential interference with the observed kinetics of reaction 1. Ethyl radicals produced in the reaction of Cl with ethane were observed directly, with their kinetics being that of slow decay, primarily due to heterogeneous wall loss. A relatively minor channel of consumption of C_2H_5 is thermal decomposition, with rate constants ranging from 2 to 34 s^{-1}, depending on the temperature and the bath gas density (values calculated from the parametrization of ref 13). Reaction of H atoms with 2,3-dichloropropene can, in principle, regenerate CH_2CClCH_2 radicals. The rate constant of the H + 2,3-$C_3H_4Cl_2$ → HCl + CH_2CClCH_2 reaction can be estimated as 7×10^{-11} exp(−2937 K/T) by analogy with the H + CCl_4 → HCl + CCl_3 reaction, which has a similar reaction enthalpy and the rate constants of which are known.[14] Thus, pseudo-first-order rates of CH_2CClCH_2 regeneration via the H + 2,3-$C_3H_4Cl_2$ are expected to be in the 2−17 s^{-1} range under the conditions of the experiments. However, competition with the much faster reaction of H atoms with ethane regenerating C_2H_5 radicals (pseudo-first-order rates of 580−1400 s^{-1} [15]) ensures that hydrogen atoms have no effect on the observed kinetics of CH_2CClCH_2. Ethyl radicals are expected to be inert with respect to abstraction of Cl from chlorinated hydrocarbon.[16,17] Similarly, rates of reactions of radicals of allylic type (CH_2CClCH_2 and $CH_2CHCHCl$) with ethane are expected to be negligible under the experimental conditions of the current study.[18]

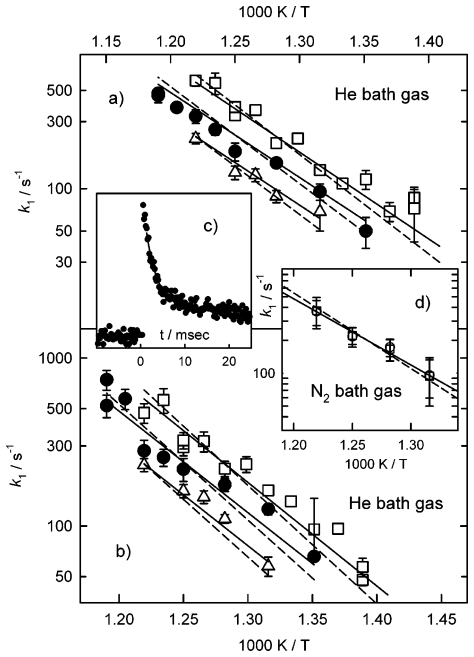

Figure 1. Plots of the CH_2CClCH_2 decomposition rate constants (k_1 vs 1000/T) for three densities of helium and one density of nitrogen: [He] = 3×10^{16} molecule cm^{-3}, triangles; [He] = 6×10^{16} molecule cm^{-3}, circles; [He] = 12×10^{16} molecule cm^{-3}, squares; [N_2] = 6×10^{16} molecule cm^{-3}, circles and squares. (a) Rate constant values (k_1-(I)) obtained in He bath gas using data fitting with floated F_R. (b) Rate constant values (k_1(II)) obtained in He bath gas using data fitting with fixed $F_R = 0.127$. (c) An example of the $C_3H_4Cl^+$ decay profile: [He] = 6×10^{16} molecule cm^{-3}, T = 830 K, k' = 394 s^{-1}, k_5 = 7.2 s^{-1}, F_R = 0.188. (d) Rate constant values obtained in N_2 bath gas: k_1(I), circles; k_1(II), squares. Lines represent the results of master equation simulation with the optimized $\langle \Delta E \rangle_{down}$ = constant (solid lines) and $\langle \Delta E \rangle_{down} = \alpha T$ (dashed lines) models.

II.2. Experimental Results. The results of all the experiments and the conditions used to determine k_1 are given in Table 1. The unimolecular rate constants for reaction 1 obtained from these sets of experiments conducted at three different densities of helium ((3, 6, and 12) $\times 10^{16}$ atom cm^{-3}) and one density of nitrogen (6×10^{16} molecule cm^{-3}) are shown in Figure 1. The CH_2CClCH_2 detection sensitivity was lower when nitrogen was used as a bath gas and k_1 values in this case could be determined only under optimal conditions.

Fitting of the $C_3H_4Cl^+$ signal profiles with eq I provided the values of F_R, the ratio of the initial intensities of the two components of the signal at mass 75 attributed to different isomers of the chloroallyl radical. The range of the fitted F_R

TABLE 1: Conditions and Results of Experiments to Determine the Rate Constants k_1 of the Unimolecular Decomposition of CH_2CClCH_2

[M][a]	T/K	[RCl][b]	$[R]_0$[b]	$[C_2H_6]$[c]	I[d]	k_3/s^{-1}	k_5/s^{-1}	F_R[e]	k_1(I) [f]/s^{-1}	k_1(II) [f]/s^{-1}
					He Bath Gas					
3.0	760	29.2	1.60	1.93	11.1	13.9	1.7	0.177 ± 0.057	68.6 ± 18.6	57.8 ± 7.6
3.0	780	34.6	1.55	2.10	9.2	16.5	2.8	0.067 ± 0.022	88.2 ± 8.8	110.4 ± 6.6
3.0	790	38	1.35	1.77	7.4	18.5	1.8	0.082 ± 0.018	125.2 ± 13.2	148.9 ± 12.9
3.0	800	34.7	1.82	1.86	11.1	16.1	2.0	0.066 ± 0.019	130.3 ± 14.4	161.9 ± 14.8
3.0	820	38	1.30	1.77	7.4	18.5	2.6	0.100 ± 0.008	227.3 ± 19.2	231.4 ± 20.6
6.0	740	30.8	1.44	2.59	9.2	14.6	5.1	0.023 ± 0.072	49.9 ± 12.3	65.8 ± 80.4
6.0	760	30.1	1.65	2.54	11.1	20.9	6.4	0.056 ± 0.026	95.2 ± 12.6	126.0 ± 9.4
6.0	780	27	1.45	2.55	11.1	20.0	3.6	0.074 ± 0.010	152.4 ± 12.0	176.4 ± 15.8
6.0	800	28.8	1.41	2.51	10.4	13.5	6.1	0.040 ± 0.017	184.0 ± 27.0	218.1 ± 33.7
6.0	810	30.8	1.33	2.59	9.2	14.6	5.1	0.104 ± 0.008	263.0 ± 23.1	256.4 ± 29.9
6.0	820	28.8	1.38	2.51	10.4	13.5	4.2	0.086 ± 0.009	327.7 ± 36.6	280.3 ± 43.7
6.0	830	56.3	0.95	2.38	3.7	16.3	7.2	0.188 ± 0.008	377.8 ± 25.9	572.5 ± 79.5
6.0	840	27	1.36	2.55	11.1	20.0	5.1	0.144 ± 0.013	460.0 ± 51.6	522.1 ± 80.2
6.0	840	65.7	1.10	2.37	3.7	17.9	7.7	0.202 ± 0.012	476.7 ± 39.7	744.2 ± 100.7
12.0	720	14.3	1.23	2.60	16.6	12.4	4.6	0.292 ± 0.027	86.2 ± 12.6	47.7 ± 3.6
12.0	720	14.3	0.55	2.60	7.4	12.4	4.6	0.199 ± 0.102	72.0 ± 30.2	57.1 ± 7.2
12.0	730	28.9	1.91	2.63	12.9	28.2	7.1	0.038 ± 0.036	69.0 ± 10.7	96.4 ± 6.9
12.0	740	14.3	1.20	2.60	16.6	13.6	5.4	0.172 ± 0.017	116.5 ± 17.9	95.6 ± 6.4
12.0	750	61.1	3.96	3.12	12.9	18.6	0.4	0.064 ± 0.011	108.7 ± 7.5	140.2 ± 8.2
12.0	760	29.8	2.73	2.65	18.5	22.5	5.6	0.077 ± 0.009	135.7 ± 10.2	163.0 ± 9.9
12.0	770	112	3.16	3.12	5.8	18.7	3.7	0.091 ± 0.008	227.5 ± 18.6	233.4 ± 25.3
12.0	780	29.6	2.12	2.84	14.8	20.3	4.2	0.076 ± 0.006	211.0 ± 14.4	219.7 ± 22.8
12.0	790	14.6	0.91	2.59	12.9	16.1	4.9	0.089 ± 0.007	362.2 ± 30.1	319.9 ± 43.6
12.0	800	29.6	2.08	2.84	14.8	21.0	2.7	0.091 ± 0.006	380.8 ± 20.7	323.8 ± 35.9
12.0	800	30.8	2.27	1.35	15.5	19.9	3.0	0.087 ± 0.005	332.6 ± 23.3	295.0 ± 33.4
12.0	810	15.5	0.94	2.61	12.9	13.5	10.5	0.126 ± 0.022	565.0 ± 99.0	563.5 ± 94.5
12.0	820	29.6	2.03	2.84	14.8	20.9	2.2	0.095 ± 0.009	587.1 ± 50.4	472.4 ± 63.2
					N_2 Bath Gas					
6.0	760	48.8	1.34	2.43	5.5	19.3	12.6	0.120 ± 0.042	93.7 ± 17.8	95.8 ± 8.7
6.0	780	48.8	1.31	2.43	5.5	15.8	6.4	0.111 ± 0.010	163.0 ± 13.3	173.2 ± 11.9
6.0	800	65.8	1.15	2.30	3.7	15.7	3.9	0.080 ± 0.008	199.4 ± 15.9	216.8 ± 20.5
6.0	820	66.4	1.14	2.29	3.7	19.9	10.1	0.109 ± 0.009	403.8 ± 43.0	367.1 ± 61.6

[a] Concentration of the bath gas (helium or nitrogen) in units of 10^{16} molecule cm^{-3}. [b] In units of 10^{11} molecule cm^{-3}. The CH_2CClCH_2 (R) concentrations were obtained by measuring the photolytic depletion of CH_2CClCH_2Cl (RCl) and represent an upper limit because they were obtained assuming a 100% yield of CH_2CClCH_2 in the photolysis. [c] In units of 10^{15} molecule cm^{-3}. [d] Estimated photolyzing laser intensity in mJ $pulse^{-1}$ cm^{-2}. [e] The ratio I_1/I_2 (eq I). [f] k_1(I) and k_1(II) were obtained using floated and fixed F_R values, respectively (see text). Error limits represent sums of 1σ random and estimated systematic uncertainties.

values is from 0.02 to 0.29. Although the exact mechanism of formation of 1-chloroallyl radicals in the photolysis of 2,3-dichloropropene is unknown, it is reasonable to expect that the ratio of the yields of the 2-chloroallyl (channels 2a and 2b) and the 1-chloroallyl (channel 2c) radicals should not depend on the conditions in the reactor within the experimental ranges. Although a minor temperature dependence can be expected in principle, its effect should be negligible considering the narrow temperature interval of the experimental study and the large amount of energy deposited in the precursor molecule by a 193 nm photon. Therefore, an alternative approach to data fitting was also implemented. In this alternative approach, a fixed value of $F_R = 0.127$ (obtained by averaging the values obtained in experiments where the relative uncertainty of fitted F_R was less than 10%) was used. The resultant values of k_1 are presented in Table 1 and Figure 1 as k_1(II); the values obtained in fitting with floated F_R are presented as k_1(I). As can be seen from the plots (a) and (b) in Figure 1, the two alternative approaches to data fitting result in somewhat different values of the rate constants. The scatter of data in the k_1 vs $1000/T$ plots is comparable in the cases of k_1(I) and k_1(II). In the absence of an objective criterion for selecting either the k_1(I) or the k_1(II) data set, both of these data sets were used in modeling the kinetics of reactions 1 and -1 (Section III).

In evaluation of the experimental uncertainties in the obtained values of k_1, effects of uncertainties in k_3 and k_5 and in the extrapolation of the nonexponential signals to zero time were taken into account. The error limits of the k_1(I) and k_1(II) values in Table 1 represent sums of 1σ statistical and estimated systematic uncertainties. It should be noted that these uncertainty values were obtained within the framework of a particular approach to data treatment, i.e., varied F_R or F_R = constant. The differences between k_1(I) and k_1(II) at individual experimental temperatures provide an additional component of uncertainty.

The values of k_1 increase with pressure; the k_1 vs pressure dependence at each particular temperature is somewhat weaker than proportional. Thus, reaction 1 is in the falloff region under the conditions of the current study. C_3H_4 was observed as a primary product of reaction 1. The $C_3H_4^+$ signal profile consisted of two components: an immediate "jump" following the photolyzing laser pulse, which can be attributed to the formation of C_3H_4 in the photolysis channel 2d, and a smaller slower-growing component, attributed to the formation of allene in reaction 1. The characteristic rise time of the second $C_3H_4^+$ signal component matched that of the CH_2CClCH_2 decay due to thermal decomposition.

III. Model of Reaction 1

III.1. Potential Energy Surface. The potential energy surface (PES) of the reactive system of CH_2CClCH_2 decomposition and the corresponding reverse reaction, that of addition of Cl to allene, was studied previously by Hudgens and Gonzalez.[19] These authors have demonstrated, using a variety of quantum chemical techniques, that the Cl atom adds to allene at the

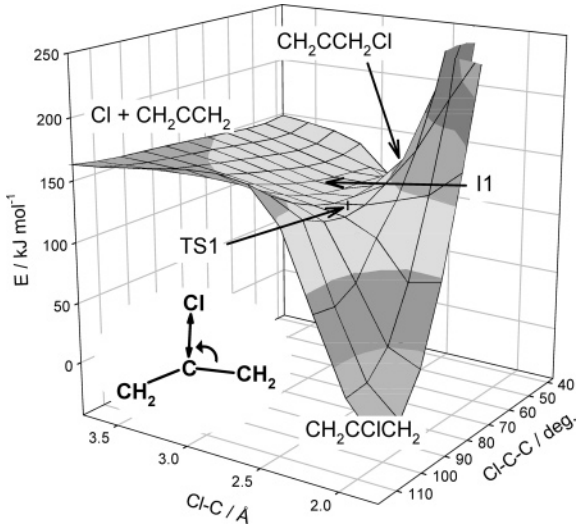

Figure 2. Three-dimensional surface plot obtained in a relaxed scan of the PES of reaction 1 using the BH&HLYP/6-311G(d,p) method. The minimum energy path of the CH_2CClCH_2 dissociation to Cl + CH_2CCH_2 proceeds from the CH_2CClCH_2 equilibrium structure through the saddle point TS1 (indicated by a short vertical dash) and the I1 plateau. The inset on the left shows the coordinates scanned: the C−Cl distance and the Cl−C−C angle.

central carbon atom, forming the 2-chloroallyl radical; initial addition at the terminal C atom results in the formation of an unstable CH_2CCH_2Cl radical that rapidly isomerizes to CH_2CClCH_2. The $CH_2CCH_2Cl \rightarrow CH_2CClCH_2$ isomerization reaction path proceeds through the PES region with an energy lower than that of the separated Cl and C_3H_4 and involves a 90° rotation of the $-CH_2$ group being formed from the chloromethyl group of CH_2CCH_2Cl. Details of the isomerization reaction path varied depending on the quantum chemical method−basis set combination used; however, the main PES and reaction path features were independent of the computational approach.

The study of the PES of reaction 1 undertaken in the current work was based on the results of Hudgens and Gonzalez. Whereas the authors of ref 19 were principally interested in the qualitative mechanism and energetics of the addition reaction, the current work concentrated on the PES properties most relevant to numerical modeling of the kinetics of the CH_2CClCH_2 decomposition, reaction 1, and the reverse reaction, −1.

Three combinations of method and basis sets were used for optimization of molecular structures: BH&HLYP/6-311G(d,p), BH&HLYP/aug-cc-pVTZ, and QCISD/6-31+G(d,p).[20−25] In addition, higher-level single-point calculations were performed at selected critical points using the QCISD(T)[23] method with the large 6-311++G(3df,2pd) basis set; QCISD(T)/6-311+G(2df,2p) energies were also calculated for the QCISD-optimized structures. The version of the BH&HLYP functional[20,21] implemented in the Gaussian 98[24] suite of programs (used in all quantum chemical calculations) was used.

A two-dimensional scan of the PES was performed at the BH&HLYP/6-311G(d,p) level. The Cl−C distance (where C is the central carbon atom) and the Cl−C−C angle (indicated with arrows in the inset in Figure 2) were scanned with the rest of the coordinates optimized. The results of the scan are shown in Figure 2. The PES obtained has three distinct regions. A minimum at Cl−C = 1.76 Å and Cl−C−C = 117° represents the 2-chloroallyl radical, CH_2CClCH_2. Another minimum at Cl−C = 2.73 Å and Cl−C−C = 38° corresponds to the CH_2CCH_2Cl isomer. These two minima are joined by a plateau

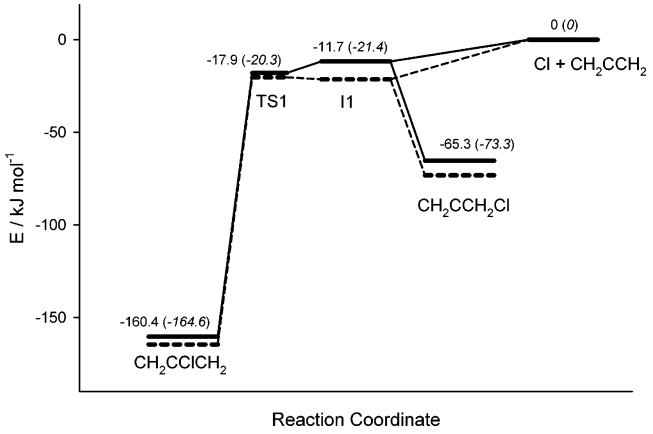

Figure 3. Potential energy diagram of reaction 1 obtained in QCISD(T)/6-311++G(3df,2pd)//QCISD/6-31+G(d,p) calculations. Energies with ZPE included are represented with solid lines and numbers outside parantheses; electronic energies (without ZPE) are represent by dashed lines and numbers in parentheses.

TABLE 2: Energies[a] of PES Stationary Points Obtained in Quantum Chemical Calculations

method[b]	E_1[c]	E_0[d]	E(I1)[e]	E_2[f]
BH	133.5 (130.2)	153.5 (149.3)		104.3 (101.8)
QCT2//BH	144.4 (141.0)	169.6 (165.4)		
BHZ	137.2 (134.0)	155.5 (151.2)		105.4 (103.3)
QCT2//BHZ	144.4 (141.2)	169.9 (165.6)		
QC	148.0 (146.2)	143.1 (138.9)	140.4 (145.9)	92.4 (96.1)
QCT1//QC	140.4 (138.6)	158.3 (154.1)	140.0 (145.5)	91.0 (94.8)
QCT2//QC	144.3 (142.5)	164.6 (160.4)	143.2 (148.7)	91.3 (95.1)

[a] Electronic energies in kJ mol^{-1}, relative to CH_2CClCH_2. Values in parentheses include added ZPE. [b] Abbreviations: BH = BH&HLYP/6-311G(d,p); BHZ = BH&HLYP/aug-cc-pVTZ; QC = QCISD/6-31+G(d,p); QCT1 = QCISD(T)/6-311+G(2df,2p); QCT2 = QCISD(T)/6-311++G(3df,2pd). [c] Energy of the TS1 saddle point. [d] Energy of Cl + CH_2CCH_2. A correction of −0.0013382 hartree is added to account for the spin−orbit energy. [e] Energy of the I1 intermediate (PES plateau). [f] Energy of the CH_2CCH_2Cl isomer.

denoted as I1 (Intermediate 1). The I1 plateau is connected with the Cl + CH_2CCH_2 valley by a wide barrierless incline; a saddle point (TS1, indicated with a short vertical dash) separates the I1 region and the CH_2CClCH_2 minimum.

The minimum energy path for the decomposition of the 2-chloroallyl radical thus proceeds from the equilibrium structure of CH_2CClCH_2 through a saddle point to the I1 plateau, with subsequent departure of Cl from allene. Another reaction path leading from the I1 plateau proceeds to the CH_2CCH_2Cl well. The well depth of CH_2CCH_2Cl is only 54 kJ mol-[1] relative to I1 and thus CH_2CCH_2Cl can be expected to be unstable and favor isomerization back to CH_2CClCH_2. The PES along the minimum energy path for reaction 1 is illustrated in Figure 3, where solid lines are used to show the energies obtained at the QCISD(T)/6-311++G(3df,2pd)//QCISD/6-31+G(d,p) level with the QCISD/6-31+G(d,p) zero-point energies (ZPE) included and dashed lines are used to show the energies obtained at the same level of calculations without the ZPE. Energies of stationary points obtained at different levels of calculations are presented in Table 2.

There is a significant degree of uncertainty associated with the part of the PES corresponding to the I1 intermediate. Although all quantum chemical method/basis set combinations used in the calculations predict the existence of the TS1 saddle point, they differ with respect to the I1 intermediate. Molecular structure optimization at the QCISD/6-31+G(d,p) level yields a shallow PES minimum but calculations performed using the

BH&HLYP density functional method do not result in a stable structure: no barrier was obtained with both the 6-311G(d,p) and the aug-cc-pVTZ basis sets for the reaction path leading from the I1 plateau to the CH_2CCH_2Cl minimum. The electronic energy difference between TS1 and I1 is very small (TS1 is 1.1 kJ mol^{-1} higher) at the QCISD(T)/6-311++G(3df,2pd)//QCISD/6-31+G(d,p) level. As a result, addition of ZPE reverses the relative positions of TS1 and I1: I1 becomes higher by 6.2 kJ mol^{-1}. At the QCISD/6-31+G(d,p) level used in structure optimization, the same TS1−I1 difference in the electronic energies is larger (7.6 kJ mol^{-1}) and addition of ZPE does not reverse the relative positions of TS1 and I1. At the BH&HLYP/6-311G(d,p) level used in the scan presented in Figure 2, there is no PES minimum for I1 but the electronic energies on the I1 plateau are $\sim 0-10$ kJ mol^{-1} lower than that of TS1. The ZPE of I1 also has a substantial uncertainty originating in the vibrational modes corresponding to C−Cl stretch and Cl−C−C bend. As can be seen from the PES plot in Figure 2, the I1 plateau is almost flat, which means that the force constants for these two types of motion are very small; however, the normal-mode analysis yields the values of 119 and 179 cm^{-1} for the corresponding vibrational frequencies. The detailed results of the quantum chemical calculations are presented in the Supporting Information.

The results of the current PES study are in agreement with those of Hudgens and Gonzalez.[19] Larger basis sets and a different DFT functional were used in the current work, which resulted in somewhat different values for the energies of the stationary points. The authors of ref 19 also observed the sensitivity of the PES details to the method/basis set combination in the region of I1 and TS1: the density functional B3LYP based structure optimization did not yield a PES minimum for I1, although the MP2 and the QCISD optimizations produced such minima and the corresponding saddle points for isomerizations to CH_2CCH_2Cl.

III.2. Rate Constant Calculations. A model of reactions (1, −1) was created on the basis of the results of quantum chemical calculations and the experimental data of the current study. QCISD/6-31+G(d,p)-level structures and frequencies were used for all species. The saddle point TS1 connecting the equilibrium CH_2CClCH_2 structure and the I1 intermediate (PES plateau) was taken as the dynamic bottleneck (transition state) of the reaction. This is a reasonable assumption considering the fact that further chemical transformation of I1 can be expected to largely favor dissociation via a very "loose"[26] complex rather than reassociation to form CH_2CClCH_2 through a "tighter" transition state. At the same time, it should be noted that trajectories originating from the CH_2CClCH_2 well and passing through the I1 region on the PES can proceed to the Cl + CH_2CCH_2 valley only if their corresponding energies are above that of Cl + CH_2CCH_2. Trajectories with energies between those of TS1 and Cl + CH_2CCH_2 will traverse the I1 plateau and will likely dwell for a limited time in the shallow CH_2CCH_2Cl well but will eventually return to the CH_2CClCH_2 well. Thus, the values of the microcanonical energy-dependent rate constants for CH_2CClCH_2 decomposition ($k(E)$) were given zero values at energies below that of Cl + CH_2CCH_2. At energies above that of Cl + CH_2CCH_2, $k(E)$ values were calculated using the RRKM method.[27−30] The sum-of-states and the density-of-states functions of the transition state and the CH_2CClCH_2 molecule, respectively, were calculated using the modified Beyer−Swinehart algorithm.[31] One rotational degree of freedom in both the transition state and the CH_2CClCH_2 molecule was taken as active.[27−30] To approximately account for the conservation of angular momentum, $k(E)$ values were multiplied by the ratio of the moments of inertia of the remaining adiabatic rotational degrees of freedom.

Pressure- and temperature-dependent rate constants of CH_2CClCH_2 decomposition were calculated via solution of a steady-state master equation[29] using the Nesbet algorithm.[32] It was demonstrated that the calculated rate constant values did not depend on the size of the energy increment (20 cm^{-1} used in the master equation solution with 2 cm^{-1} used in $k(E)$ calculations) used in converting the continuous form of the master equation into the matrix form.[29] It was also demonstrated that solution of the full time-dependent master equation[29] performed using the Householder tridiagonalization algorithm (see refs 33 and 34 for details) resulted in the same rate constant values as were obtained with the steady-state master equation. The *ChemRate* program[35] was used in all calculations.

The exponential-down[29,36] model of collisional energy transfer was used in the calculations. The values of the collisional energy transfer parameter, $\langle\Delta E\rangle_{down}$ (average energy transferred per deactivating collision with the bath gas), is unknown and can only be obtained from fitting of the experimental data. However, this parameter, generally, has an unknown temperature dependence. Two models of the $\langle\Delta E\rangle_{down}$ vs temperature dependence for CH_2CClCH_2 were used in the current study. The first model employed a temperature-independent $\langle\Delta E\rangle_{down}$ = constant. The second model used a proportional $\langle\Delta E\rangle_{down} = \alpha T$ dependence, based on analogy with the results of Knyazev and Tsang obtained for *s*-C_4H_9.[37] These authors modeled the chemically and thermally activated decomposition of *s*-C_4H_9 to reproduce the experimental literature data obtained over a wide range of temperatures (195−680 K). The modeling yielded $\langle\Delta E\rangle_{down}$ proportional to temperature: $\langle\Delta E\rangle_{down}(s\text{-}C_4H_9,He) = 0.52T$ cm^{-1} K^{-1}. A similar proportional dependence was obtained earlier for the decomposition of ethyl radical.[13,38]

As a starting point in the calculations, the values of the energy of the TS1 saddle point (E_1) and that of the Cl + CH_2CCH_2 threshold (E_0) obtained in the QCISD(T)/6-311++G(3df,2pd)//QCISD/6-31+G(d,p) calculations were used. Then, critical parameters of the model were adjusted to achieve agreement with the rate constants of reaction 1 obtained in the current work and those of reaction −1 reported in refs 6−8. The results of the calculations demonstrate different sensitivities to different model parameters, depending on the temperature and pressure values selected for calculations. The near-high-pressure-limit rate constant at room temperature (the k_{-1} value of ref 6) is most sensitive to two parameters: $E_1 - E_0$, the energy difference between TS1 and the Cl + CH_2CCH_2 products, and the vibrational frequencies of the transition state. The low-pressure (5−10 Torr) values of k_{-1} obtained from the results of Farrell and Taatjes[7] and those reported by Atkinson and Hudgens[8] are most sensitive to $E_1 - E_0$, $\langle\Delta E\rangle_{down}$, and the CH_2CClCH_2 well depth, E_0. The rate constants k_1 of the CH_2CClCH_2 decomposition at the low pressures used in the experimental part of the current study are most sensitive to E_0 and $\langle\Delta E\rangle_{down}$ and are not sensitive to either $E_0 - E_1$ or the TS1 vibrational frequencies. Because variations in $E_0 - E_1$ and in the vibrational frequencies of TS1 lead to the same result, i.e., changes in the calculated high-pressure-limit values of k_{-1}, the frequencies of the transition state were fixed at the values obtained in QCISD/6-31+G(d,p) calculations. Thus, the following parameters were optimized in the modeling: (1) $E_1 - E_0$, (2) E_0, (3) $\langle\Delta E\rangle_{down}(CO_2)$ (for CO_2 bath gas used in ref 7), and (4) $\langle\Delta E\rangle_{down}$(He). Optimization was performed twice, using the $\langle\Delta E\rangle_{down}$ = constant and the $\langle\Delta E\rangle_{down} = \alpha T$ models. The values of $\langle\Delta E\rangle_{down}$-

TABLE 3: Results of Modeling of the Experimental k_1 and k_{-1} Data

model parameter	$\langle\Delta E\rangle_{down}$ = const[a]	$\langle\Delta E\rangle_{down} = \alpha T^b$	QCISD(T)[c]
E_1/kJ mol^{-1}	144.3	151.4	142.5
E_0/kJ mol^{-1}	161.4	168.5	160.4
$\langle\Delta E\rangle_{down}(CO_2)$[d]/cm^{-1}	1402	1.586T/K	
$\langle\Delta E\rangle_{down}$(He)/cm^{-1}	174	0.434T/K	
$\langle\Delta E\rangle_{down}(N_2)$/cm^{-1}	221	0.572T/K	

[a] Values obtained using the $\langle\Delta E\rangle_{down}$ = constant model (preferred model). [b] Values obtained using the $\langle\Delta E\rangle_{down} = \alpha T$ model. [c] Energy values obtained in the QCISD(T)/6-311++G(3df,2pd)//QCISD/6-31+G(d,p) calculations with ZPE included. [d] The same $\langle\Delta E\rangle_{down}$ values were used for ethane bath gas.

(N_2) were then obtained from fitting both the k_1 data (current study) and the value of k_{-1} at 5 Torr of N_2 reported in ref 8. In the experimental part of the current work, nonnegligible concentrations of ethane (2−6% of the total pressure) were used. In the absence of any other information on $\langle\Delta E\rangle_{down}$ for collisions between the 2-chloroallyl radical and ethane, the values of $\langle\Delta E\rangle_{down}(CO_2)$ obtained in the fitting of the k_{-1} data of ref 7 were used for the ethane bath gas.

The value of k_{-1} at 295 K and 760 Torr of N_2 reported in ref 6 was obtained in a relative rates experimental study. For the purpose of the modeling, this value was reevaluated in the current work using a newer value[39] for the rate constant of the reference reaction, that of Cl with n-C_4H_{10}. The reevaluated value of k_{-1} is $(4.19 \pm 0.45) \times 10^{-10}$ cm^3 molecule^{-1} s^{-1}.

The use of the QCISD(T)/6-311++G(3df,2pd)//QCISD/6-31+G(d,p) based values of E_1 and E_0 results in $k_{-1} = 5.12 \times 10^{-10}$ cm^3 molecule^{-1} s^{-1} for the conditions of Wallington et al.,[6] which is outside the error limits of the experimental value by only 10%. Increasing the value of E_1 by only 0.8 kJ mol^{-1} (to achieve $E_1 - E_0 = -17.1$ kJ mol^{-1}) brings the calculated value of k_{-1} into agreement with experiment. Fitting of other model parameters was performed by minimizing the sums of squares of deviations between the calculated and the experimental rate constant values weighted proportionally to the inverse squares of the experimental uncertainties. The values of E_1, E_0, $\langle\Delta E\rangle_{down}(CO_2) = \langle\Delta E\rangle_{down}(C_2H_6)$, $\langle\Delta E\rangle_{down}$(He), and $\langle\Delta E\rangle_{down}(N_2)$ obtained in optimization of models with $\langle\Delta E\rangle_{down}$ = constant and $\langle\Delta E\rangle_{down} = \alpha T$ temperature dependences are given in Table 3. Use of the two different models for $\langle\Delta E\rangle_{down}$ temperature dependence yields optimized energy values (E_1 and E_0) that differ by 7.1 kJ mol^{-1}.

Figure 4 presents the agreement between the experimental values of k_{-1} (symbols) and those obtained in calculations with the model optimized using the $\langle\Delta E\rangle_{down}$ = constant constraint. In Figure 1, the calculated $k_1(T)$ dependences (lines) are displayed together with the experimental k_1 values, with the solid lines representing the $\langle\Delta E\rangle_{down}$ = constant model and the dashed lines the $\langle\Delta E\rangle_{down} = \alpha T$ model. The scatter of the experimental k_1 values in the Arrhenius plots in Figure 1 is too large to allow an accurate determination of the activation energy and the reaction energy threshold. However, comparison of the $k_1(T)$ dependences predicted by the two models demonstrates that the $\langle\Delta E\rangle_{down} = \alpha T$ model noticeably overestimates the Arrhenius slopes, whereas the slopes resulting from the $\langle\Delta E\rangle_{down}$ = constant model are in general agreement with experiment. We select for further use the $\langle\Delta E\rangle_{down}$ = constant model. The differences between the predictions of the two models are then taken as a representation of the model uncertainties.

III.3. Parametrization of the Rate Constants. We present here a parametrization of k_1 and k_{-1} in helium and nitrogen, which provides rate constant values throughout the range of

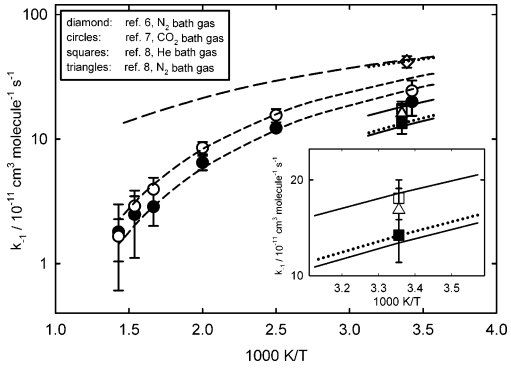

Figure 4. Experimental (symbols) and calculated (lines) rate constants of reaction −1. Experimental data are from refs 6 (diamond), 7 (filled circles, 5 Torr of CO_2; open circles, 10 Torr of CO_2), and 8 (filled square, 5 Torr of He; open square, 10 Torr of He; triangle, 5 Torr of N_2). Lines are the results of modeling with the $\langle\Delta E\rangle_{down}$ = constant model: long-dash dashed line, the high-pressure-limit rate constants; short-dash dashed lines, $k_1(T)$ for the conditions of ref 7 (5 and 10 Torr of the CO_2 bath gas); solid lines, $k_1(T)$ for the conditions of ref 8 in He bath gas (5 and 10 Torr); dotted lines, $k_1(T)$ for N_2 bath gas under the conditions of refs 8 (5 Torr) and 6 (760 Torr). The inset enlarges the part of the plot showing the k_1 values of ref 8 and the corresponding calculated lines.

temperatures 300−1600 K and pressures 1 to 1×10^4 Torr. The modified Lindemann−Hinshelwood expression introduced by Gilbert et al.[40] was used. Values of k_1 and k_{-1} in the above temperature and pressure intervals were calculated using the master equation/RRKM approach with the optimum model of the reaction presented above (Table 3). The following temperature dependences of the high- and the low-pressure-limit rate constants were obtained:

$$k^{\infty}_{1} = 1.45 \times 10^{20} T^{-1.75} \exp(-19609\ \mathrm{K}/T)\ \mathrm{s}^{-1} \quad \text{(II)}$$

$$k^{\infty}_{-1} = 8.94 \times 10^{-10} T^{-0.40} \exp(481\ \mathrm{K}/T)\ \mathrm{cm}^3\ \mathrm{molecule}^{-1}\ \mathrm{s}^{-1} \quad \text{(III)}$$

$$k_1^{0}(\mathrm{He}) = 5.01 \times 10^{-32} T^{-12.02} \exp(-22788\ \mathrm{K}/T)\ \mathrm{cm}^3\ \mathrm{molecule}^{-1}\ \mathrm{s}^{-1} \quad \text{(IV)}$$

$$k_1^{0}(\mathrm{N_2}) = 2.50 \times 10^{-32} T^{-11.92} \exp(-22756\ \mathrm{K}/T)\ \mathrm{cm}^3\ \mathrm{molecule}^{-1}\ \mathrm{s}^{-1} \quad \text{(V)}$$

The matrix of calculated values of rate constants was fitted with the modified Lindemann−Hinshelwood expression and the resulting temperature dependences of F_{cent} (general center broadening factor[40]) can be represented with the following expressions:

$$F_{cent}(\mathrm{He}) = 0.46 \exp(-T/1001\ \mathrm{K}) + 0.54 \exp(-T/996\ \mathrm{K}) + \exp(-4008\ \mathrm{K}/T) \quad \text{(VI)}$$

$$F_{cent}(\mathrm{N_2}) = 0.37 \exp(-T/2017\ \mathrm{K}) + 0.63 \exp(-T/142\ \mathrm{K}) + \exp(-4812\ \mathrm{K}/T) \quad \text{(VII)}$$

The average deviation of fit is 3% and the maximum deviation is 22% (observed at the lowest pressure−highest temperature combination). The upper temperature limit of the rate constant parametrization is determined by the significance of non-steady-state effects[34,41−45] above 1600 K where the notion of a time-independent rate constant is inapplicable and the formalism of virtual components[45] must be used if an accurate description of unimolecular kinetics as a part of complex combustion kinetics

is desired. Already at 1600 K, non-steady-state effects can be observed: in the case of an initial Boltzmann distribution of CH_2CClCH_2, the first 20% of molecules decompose with an effective rate constant that is more than twice as large as the steady-state rate constant.

The influence of model uncertainty (represented by the difference between the $\langle\Delta E\rangle_{down}$ = constant and the $\langle\Delta E\rangle_{down} = \alpha T$ models) on the rate constants of reactions 1 and −1 was evaluated. The resultant uncertainty factors for the high-pressure-limit rate constants of reaction 1 are 17 at 300 K, 5 at 500 K, 3 at 800 K, 2 at 1200 K, and 1.7 at 1600 K. The high-pressure-limit rate constants of the reverse reaction are not affected by the choice of the model because the values of k^{∞}_{-1} are not sensitive to the CH_2CClCH_2 well depth. The uncertainty factors obtained for the falloff region are tabulated in the Supporting Information.

IV. Discussion

The current study provides the first experimental determination of the rate constants of reaction 1. The values of k_1 were obtained as a function of temperature and bath gas density in two bath gases, helium and nitrogen. No previous experimental or computational studies of the kinetics of this reaction exist in the literature. Such lack of experimental and computational information is rather typical for many of the reactions involving chlorinated hydrocarbon radicals. This absence of experimental data increases the relevance of computational methods that can be used for assessing kinetic parameters. In this respect, it is interesting to compare the results of the potential energy surface (PES) study performed in the current work with the properties of PES derived from the experiment.

The minimum energy path of reaction 1 proceeds from the equilibrium structure of CH_2CClCH_2 through a saddle point to the shallow attractive complex (PES plateau, intermediate I1), with subsequent barrierless departure of the chlorine atom to form the $Cl + CH_2CCH_2$ products, as described in section III (Figure 2). This reaction mechanism is qualitatively similar to those observed for other reactions of decomposition of chlorinated hydrocarbon radicals where reactions occur via elimination of a chlorine atom and formation of a π bond: $CH_2CH_2Cl \rightarrow C_2H_4 + Cl$[46,47] and $C_2Cl_3 \rightarrow Cl + C_2Cl_2$.[48] In these reactions, the minimum energy path also passes through a shallow region on the PES with energy below that of the separated products. Quantum chemical calculations demonstrate that the C_2Cl_3 PES differs from that of the CH_2CH_2Cl decomposition by the existence of a saddle point between the equilibrium configuration and that of the shallow "departure" complex. In the PES study of reaction 1, electronic energy calculations predict the existence of a similar saddle point (TS1) and yield the energy of the I1 intermediate (a PES plateau) that is lower than that of TS1. However, inclusion of the ZPE calculated at the QCISD/6-31+G(d,p) level for the I1 intermediate inverts the relative positions of TS1 and I1 (Figure 3). As discussed in section III, there is a significant degree of uncertainty associated with the part of the PES corresponding to the I1 intermediate. For example, the BH&HLYP level calculations predict deeper energy differences between TS1 and the I1 region compared to the QCISD(T)//QCISD calculations (thus suggesting that ZPE addition will not invert the relative TS1 and I1 positions) but do not yield a stationary point for I1 producing instead a barrierless reaction path between the I1 plateau and the CH_2CCH_2Cl structure. Even considering the PES uncertainties, the dynamic bottleneck of reaction 1 is likely to be located near the TS1 structure: its density of states is likely to be lower than that of the structures in the I1 plateau region because of the flatness of the I1 potential energy surface with respect to the degrees of freedom corresponding to the Cl−C stretch and the Cl−C−C bend (Figure 2).

The energies of the TS1 saddle point (E_1) and the $Cl + CH_2CCH_2$ products (E_0) relative to that of the equilibrium CH_2CClCH_2 configuration obtained in quantum chemical calculations can be compared with the values derived from modeling of the experimental data. As can be seen from Table 3, energies obtained at the QCISD(T)/6-311++G(3df,2pd)//QCISD/6-31+G(d,p) level are in remarkable agreement with those of the preferred model with the $\langle\Delta E\rangle_{down}$ = constant, with differences of only 1.8 and 1.0 kJ mol^{-1}. Calculations employing the QCISD(T) method with large basis sets and BH&HLYP-based molecular structures also give small deviations with the experiment-based model, 4.6 kJ mol^{-1} on average, which is smaller than the differences between the preferred model and that based on the $\langle\Delta E\rangle_{down} = \alpha T$ assumption (Tables 2 and 3). The BH&HLYP energies, however, have larger deviations, 11.7 kJ mol^{-1} on average.

Acknowledgment. This research was supported by the National Science Foundation, Combustion and Thermal Plasmas Program under Grant No. CTS-0105239.

Supporting Information Available: Detailed results of the quantum chemical and rate constants calculations. This material is available free of charge via the Internet at http://pubs.acs.org.

References and Notes

(1) Tsang, W. *Combust. Sci. Technol.* **1990**, *74*, 99.
(2) Taylor, P. H.; Dellinger, B. *J. Anal. Appl. Pyrol.* **1999**, *49*, 9.
(3) Taylor, P. H.; Lenoir, D. *Sci. Total Environ.* **2001**, *269*, 1.
(4) Babushok, V.; Tsang, W.; Noto, T. *Proc. Combust. Inst.* **2000**, *28*, 2691.
(5) Shestov, A. A.; Knyazev, V. D. *J. Phys. Chem. A* **2004**, *108*, 11339.
(6) Wallington, T. J.; Skewes, L. M.; Siegl, W. O. *J. Photochem. Photobiol. A* **1988**, *45*, 167.
(7) Farrell. J. T.; Taatjes, C. A. *J. Phys. Chem. A* **1998**, *102*, 4846.
(8) Atkinson, D. B.; Hudgens, J. W. *J. Phys. Chem. A* **2000**, *104*, 811.
(9) Hudgens, J. W.; Gonzalez, C. *J. Phys. Chem. A* **2002**, *106*, 1739.
(10) Slagle, I. R.; Gutman, D. *J. Am. Chem. Soc.* **1985**, *107*, 5342.
(11) Timonen, R. S.; Ratajczak, E.; Gutman, D.; Wagner, A. F. *J. Phys. Chem.* **1987**, *91*, 5325.
(12) Krasnoperov, L. N.; Niiranen, J. T.; Gutman, D.; Melius, C. F.; Allendorf, M. D. *J. Phys. Chem.* **1995**, *99*, 14347.
(13) Feng, Y.; Niiranen, J. T.; Bencsura, A.; Knyazev, V. D.; Gutman, D.; Tsang, W. *J. Phys. Chem.* **1993**, *97*, 871.
(14) Bryukov, M. G.; Slagle, I. R.; Knyazev, V. D. *J. Phys. Chem. A* **2001**, *105*, 3107.
(15) Bryukov, M. G.; Slagle, I. R.; Knyazev, V. D. *J. Phys. Chem. A* **2001**, *105*, 6900.
(16) Matheson, I.; Tedder, J. *Int. J. Chem. Kinet.* **1982**, *14*, 1033.
(17) Szirovicza, L.; Woog, J.; Bardi, I. *Acta Chim. Acad. Sci. Hung.* **1989**, *126*, 117.
(18) Tsang, W. *J. Phys. Chem. Ref. Data* **1991**, *20*, 221.
(19) Hudgens, J. W.; Gonzalez, C. *J. Phys. Chem. A* **2002**, *106*, 6143.
(20) Becke, A. D. *J. Chem. Phys.* **1993**, *98*, 1372.
(21) Lee, C. T.; Yang, W. T.; Parr, R. G. *Phys. Rev. B* **1988**, *37*, 785.
(22) Kendall, R. A.; Dunning, T. H., Jr.; Harrison, R. J. *J. Chem. Phys.* **1992**, *96*, 6796.
(23) Pople, J. A.; Head-Gordon, M.; Raghavachari, K. *J. Chem. Phys.* **1987**, *87*, 5968.
(24) Frisch, M. J.; Trucks, G. W.; Schlegel, H. B.; Scuseria, G. E.; Robb, M. A.; Cheeseman, J. R.; Zakrzewski, V. G.; Montgomery, J. A., Jr.; Stratmann, R. E.; Burant, J. C.; Dapprich, S.; Millam, J. M.; Daniels, A. D.; Kudin, K. N.; Strain, M. C.; Farkas, O.; Tomasi, J.; Barone, V.; Cossi, M.; Cammi, R.; Mennucci, B.; Pomelli, C.; Adamo, C.; Clifford, S.; Ochterski, J.; Petersson, G. A.; Ayala, P. Y.; Cui, Q.; Morokuma, K.; Malick, D. K.; Rabuck, A. D.; Raghavachari, K.; Foresman, J. B.; Cioslowski, J.; Ortiz, J. V.; Baboul, A. G.; Stefanov, B. B.; Liu, G.; Liashenko, A.; Piskorz, P.; Komaromi, I.; Gomperts, R.; Martin, R. L.; Fox, D. J.; Keith, T.; Al-Laham, M. A.; Peng, C. Y.; Nanayakkara, A.; Challacombe, M.; Gill, P. M. W.; Johnson, B.; Chen, W.; Wong, M. W.; Andres, J. L.; Gonzalez, C.;

Head-Gordon, M.; Replogle, E. S.; Pople, J. A. *Gaussian 98*, revision A.9; Gaussian, Inc.: Pittsburgh, PA, 1998.

(25) Foresman, J. B.; Frisch, A. E. *Exploring Chemistry With Electronic Structure Methods*, 2nd ed.; Gaussian, Inc.: Pittsburgh, PA, 1996.

(26) Benson, S. W. *Thermochemical Kinetics*, 2nd ed.; John Wiley and Sons: New York, 1976.

(27) Robinson, P. J.; Holbrook, K. A. *Unimolecular Reactions*; Wiley-Interscience: New York, 1972.

(28) Forst, W. *Theory of Unimolecular Reactions*; Academic Press: New York, 1973.

(29) Gilbert, R. G.; Smith, S. C. *Theory of Unimolecular and Recombination Reactions*; Blackwell: Oxford, U.K., 1990.

(30) Holbrook, K. A.; Pilling, M. J.; Robertson, S. H. *Unimolecular Reactions*, 2nd ed.; Wiley: New York, 1996.

(31) Astholz, D. C.; Troe, J.; Wieters, W. *J. Chem. Phys* **1979**, *70*, 5107.

(32) Gaynor, B. J.; Gilbert, R. G.; King, K. D. *Chem. Phys. Lett* **1978**, *55*, 40.

(33) Bedanov, V. M.; Tsang, W.; Zachariah, M. R. *J. Phys. Chem.* **1995**, *99*, 11452.

(34) Tsang, W.; Bedanov, V.; Zachariah, M. R. *J. Phys. Chem.* **1996**, *100*, 4011.

(35) Mokrushin, V.; Bedanov, V.; Tsang, W.; Zachariah, M. R.; Knyazev, V. D. *ChemRate, Version 1.19*; National Institute of Standards and Technology: Gaithersburg, MD 20899, 2001.

(36) Rabinovitch, B. S.; Tardy, D. C. *J. Chem. Phys.* **1966**, *45*, 3720.

(37) Knyazev, V. D.; Tsang, W. *J. Phys. Chem. A* **2000**, *104*, 10747.

(38) Knyazev, V. D. *J. Phys. Chem.* **1995**, *99*, 14738.

(39) Tyndall, G. S.; Orlando, J. J.; Wallington, T. J.; Dill, M.; Kaiser, E. W. *Int. J. Chem. Kinet.* **1997**, *29*, 43.

(40) Gilbert, R. G.; Luther, K.; Troe, J. *Ber. Bunsen-Ges. Phys. Chem.* **1983**, *87*, 169.

(41) Schranz, H. W.; Nordholm, S. *Chem. Phys.* **1984**, *87*, 163.

(42) Bernshtein, V.; Oref, I. *J. Phys. Chem.* **1993**, *97*, 6830.

(43) Kiefer, J. H. *Proc. Combust. Inst.* **1998**, *27*, 113.

(44) Barker, J. R.; King, K. D. *J. Chem. Phys.* **1995**, *103*, 4953.

(45) Knyazev, V. D.; Tsang, W. *J. Phys. Chem. A* **1999**, *103*, 3944.

(46) Engels, B.; Peyerimhoff, S. D.; Skell, P. S. *J. Phys. Chem.* **1990**, *94*, 1267.

(47) Knyazev, V. D.; Kalinovski, I. J.; Slagle, I. R. *J. Phys. Chem. A* **1999**, *103*, 3216.

(48) Bryukov, M. G.; Kostina, S. A.; Knyazev, V. D. *J. Phys. Chem. A* **2003**, *108*, 6574.